Available online at www.sciencedirect.com

ScienceDirect

Science and Technology of MATERIALS

http://ees.elsevier.com/stmat

Science and Technology of Materials 30 (2018) 92–98

Bioinspired shape controlled antiferromagnetic Co_3O_4 with prism like-anchored octahedron morphology: A facile green synthesis using *Manihot esculenta Crantz* extract

E.U. Ikhuoria [a,c,d,*], S.O. Omorogbe [b,c,d], B.T. Sone [c,d], M. Maaza [c,d]

[a] *Department of Chemistry, University of Benin, Benin City, Nigeria*

[b] *Product Development Laboratory, Rubber Research Institute of Nigeria, P. M. B. 1049, Benin City, Nigeria*

[c] *UNESCO-UNISA Africa Chair in Nanosciences/Nanotechnology, College of Graduate Studies, University of South Africa, Muckleneukridge, POBox 392, Pretoria, South Africa*

[d] *Nanosciences African Network (NANOAFNET), iThemba LABS-National Research Foundation, 1 Old Faure Road, Somerset West 7129, POBox 722, Somerset West, Western Cape Province, South Africa*

Received 24 November 2017; accepted 23 February 2018

Abstract

Several strategies have been established for the synthesis of cobalt oxide nanoparticles with tunable sizes, morphologies and magnetic properties that involve the use of environmentally malignant organic solvent and high temperature conditions. Herein, we report on a facile green approach to synthesize antiferromagnetic Co_3O_4 mesoscale particles, defect free with prism liked-anchored octahedron morphology. The structural and magnetic properties of the as-synthesized Co_3O_4 nanoparticles were characterized using powder X-ray diffraction (XRD), scanning electron microscopy (SEM), energy dispersive analysis (EDAX), transmission electron microscopy (TEM), thermogravimetric analysis (TGA) coupled mass (MS), Fourier transform infrared spectroscopy (FT-IR) and vibrating sample magnetometer (VSM). The structural properties indicate that the as-synthesized mesostructured Co_3O_4 particles are pure crystallites of face-centred cubic phase Co_3O_4. The Co_3O_4 mesoparticles had bandgap of 2.86 and 2.54 eV and showed antiferromagnetic behaviour.

Keywords: *Manihot esculanta Crantz* extract; Antiferromagnetic Co_3O_4; Octahedron morphology; Green synthesis

1. Introduction

The synthesis of nanosized or mesosized crystalline metal oxides is increasingly gaining research interest because of their adsorptive properties, large surface area, surface defects and fast diffusivities [1]. They exhibit novel material properties that are very different from those of their bulk counterparts due to their small sizes. It has been established that metal and metal oxides nanoparticles are capable of increasing chemical reaction activities due to the high ratio of surface atoms with free valences to the cluster of total atoms [2].

Cobalt (Co)-based nanomaterials have attracted numerous research interest because of their good electro-activity and low cost [2–4]. Cobalt is a transition metal and is capable of exhibiting variable oxidation states (Co^{2+}, Co^{3+}, Co^{4+}). This multivalent state of cobalt provides it the ability to be present in various spin states in its oxide forms: Low, high as well as intermediate spin [5]. Co_3O_4 exists as a regular spinel structure with Co^{3+} in the octahedral sites and Co^{2+} in the tetrahedral site. This is attributable to the stability of the Co^{3+} (low spin d6) in the octahedral crystal field. The presence of octahedral and tetrahedral sites in Co_3O_4 results in two-sublattices in the crystal, hence in its bulk form, Co_3O_4 is anti-ferromagnetic with a Neel temperature of 33 K [6,7]. However, unlike the bulk form, Co_3O_4 particles exhibit a weak ferromagnetic behaviour. This is consistent with early predictions by Neel who suggested that

* Corresponding author.
E-mail address: esyikhuoria@yahoo.com (E.U. Ikhuoria).

https://doi.org/10.1016/j.stmat.2018.02.003

at the nanoscale the reduced coordination of surface spins will result in a change in magnetic order making materials that are anti-ferromagnetic in their bulk form to become weakly ferromagnetic or superparamagnetic [6]. The effects of quantum confinement and surface effects and variable oxidation state of cobalt have made Co_3O_4 nanoparticles find immense applications in areas such as catalysis, intercalation compounds for energy storage in Li-ion batteries, gas sensors, electrochemical devices, pigments, high-temperature solar absorbers, magnetic materials among others [8,9].

Previous research work on Co_3O_4 focused on the synthesis of novel morphologies of the oxide and their applications. Some notable physical and chemical synthetic routes have been used in the synthesis of nanocrystalline Co_3O_4. Sol–gel synthesis, spray pyrolysis, coprecipitation, reduction, electrodeposition, chemical vapour deposition, thermal decomposition, solvothermal, microemulsion, pulsed laser deposition, sputtering, among others have been reported [8,10–15]. Though, these methods have shown varying degrees of successes in producing Co_3O_4 nanoparticles with good properties and some control over the obtained morphology, there are some drawbacks such as high cost, and dependence of particle growth kinetics on parameters such as pH, temperature, adsorption of surfactants [16]. Furthermore, some of the surfactants and stabilizers applied in the synthesis procedure tend to be hazardous with carcinogenic and cytotoxic effects making the synthesized nanomaterials unsuitable for clinical and biomedical applications. Consequently, current research interest is drifting towards green synthesis involving the use of environmentally friendly biological materials in the synthesis of nanomaterials (biosynthesis). Besides producing environmentally friendly nanostructures, biosynthetic routes provide control over the obtained morphology of particles by serving as templates for the hierarchical assembly of obtained nanostructures into complex micro, meso and macro entities [16]. Biosynthesis typically employs the use of bacteria, yeast, viruses, plants, fungus, actinomycetesetc. for the production of nanomaterials. Among these biomaterials, the use of plants provides the unique advantages of simplicity, scalability for production on a large scale. It is much faster since it does not require the complex multi-step processes of isolation, culture preparation, and culture maintenance typical in microbe-based synthesis [16]. Biosynthetic routes based on plants typically employ the phenolic, alkaloids, proteins, sugars, and terpenoids present in plants as stabilizers and reducing agents for the synthesis of the desired nanostructures. Initially, these chemicals aid the conversion of the metal precursor from their high oxidation states to zerovalent states, followed by nucleation. Growth occurs thereafter to yield nanoparticles which form aggregates based on the intermolecular interactions between the nanoparticles and the plant extracts to yield the most stable nanoparticles' morphologies [16]. The pH, concentration (of both the metal precursors and plant extracts), temperature, reaction time are among the factors that control particle shape, sizeand morphology. Some notable research efforts involving the use of plant extracts in nanoparticles synthesis have been recorded [5,17].

Manihot esculenta Crantz is a woody shrub found in South America. It has been identified as a staple food for more than 500 million people in the tropics, many of whom are very poor [18]. It is considered a major source of industrial raw material and income for rural communities in most African Countries [19,20]. However, It contains anti-nutritional cyanogenic glucosides such as Linamarin and Lotaustralin The main organ of storage of the plant is the root and it has three distinct parts: bark (Periderm), Peel (Cortex) and Parenchyma. However, the consumption of *Manihot esculenta Crantz* roots and leaves are restricted by the cyanide content. The root Parenchyma has a cyanide content ranging from 10 to 500 mg cyanide equivalent/kg dry matter [21]. In this study, we report for the first time, the use of a natural extract of *Manihtot esculenta Crantz* Parenchyma as a chelating agent in the production of magnetic cobalt oxide (Co_3O_4) for multifunctional applications.

2. Experimental

2.1. Materials

Cobalt ($CoCl_2$, 98%) was purchased from May and Baker, Dagenham, England. *Manihot esculenta Crantz* was obtained from the plantation of Rubber Research Institute of Nigeria. It was extracted before use. Type 1, Ultrapure deionized water (18.2 MΩ cm, 25 °C), Merck Millipore (Germany) was used for preparing all solutions. The chemical(s) used were of AR grade and were used as received.

2.2. Biosynthesis process of cobalt oxides particles via Manihot esculenta Crantz extract

The tuberous root parenchyma was peeled, washed with deionized water, grated and dewatered. The extract was centrifuged to remove the starch. The supernatant obtained thereof was stored at 4 °C.

In a typical experiment, 0.02 mol $CoCl_2$ was dissolved in 30 mL of *Manihot esculenta Crantz* extract for stabilization to occur. The mixture was allowed to stand for 24 h under ambient conditions. The mixture formed a precipitate which was separated using an Eppendorf centrifuge and dried in a vacuum oven at 60 °C for 24 h. The dried powder was subsequently annealed at 500 °C for 2 h (Scheme 1).

2.3. Materials characterization

Surface morphology of the prepared powders was carried out using an Auriga high-resolution scanning electron microscope (HRSEM) coupled to an Oxford Instruments Xmax solid state silicon-drift detector (20 keV) used for carrying out the elemental analysis by energy dispersive X-ray spectroscopy (EDS). High-resolution transmission electron microscopy (HRTEM) was performed in a TECNAI F2 G20 HRTEM. The sample subjected to HRTEM was obtained by drop casting on a 400 mesh Cu grid and dried under vacuum at room temperature. Electron dispersive X-ray spectroscopy (EDS) was carried out using a specialized detector coupled to an OXFORD Instruments nano-scanning electron microscope. Perkin-Elmer spectrum one FT-IR spectrometer operating between 4000 and 400 cm^{-1} was

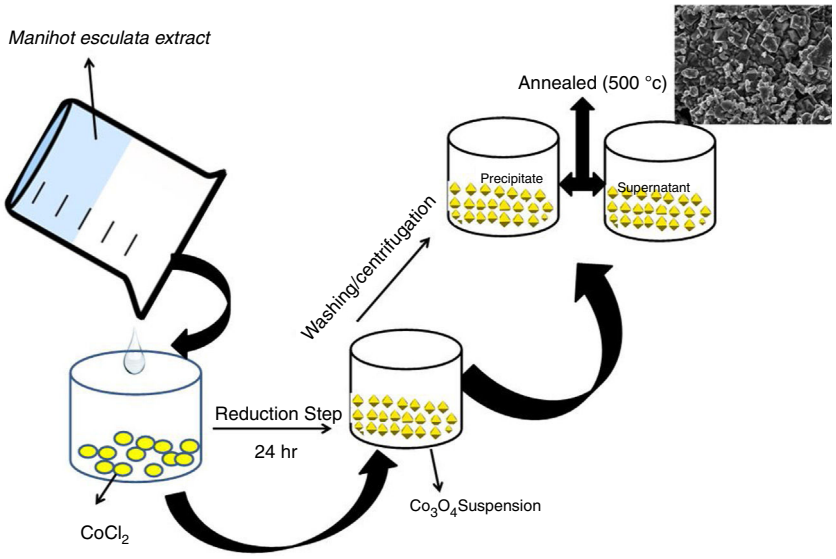

Scheme 1. Proposed schematic for the as-synthesized Co_3O_4 mesoparticles.

used to determine the vibration present in the cobalt oxide mesoparticles. A resolution of 4 cm^{-1} was used and 64 scans were performed for each spectrum. The IR spectra were recorded as KBr pellets by subtracting the spectra of the KBr from cobalt oxide nanoparticles. Cryogenic Ltd, VSM was used to measure the magnetization field sweep loop of the samples, both at 5 K and 300 K. The apparatus is a closed-loop helium cooling system installed with aNbTi superconducting magnet. The field was orientated vertically and the measurement sequence was programmed such that the settling time of 30 sec (at each point) and an average of 20 measurements were taken per data point. This was done to have high resolution and accuracy of data. The frequency of the sample between the pick-up magnets was 20 Hz and this was controlled by an optical transducer.

3. Results and discussion

The X-ray diffraction pattern of the as-synthesized Co_3O_4 mesoparticles is shown in Fig. 1a. The XRD pattern indexed to (111), (220), (311), (222), (400), (511) (440) and (620) planes corresponding to the face centre cubic phase which matched with JCPDS No. 00-042-1467 with FD- 3m (227) space group and lattice constant, $\alpha = 8.08$ A. No characteristic peaks of other impure phases were detected. This showed that the as-synthesized black powder is of high quality and highly crystalline. The XRD results further showed that the Co_3O_4 samples crystallized at a single phase but, they have different FWHM which means they have different particle sizes. The precipitated Co_3O_4 sample had higher FWHM than the supernatant as evaluated from the XRD peaks. This resulted in reduced particle size as seen from the calculated Scherrer's equation.

The crystallite size of the synthesized Co_3O_4 was determined using the Scherrer's formula Eq. (1) to be ca. 36 nm while the lattice strain is 0.0032.

$$\Delta d = \frac{K\lambda}{\beta \cos \theta} \tag{1}$$

where k is constant (ca. 0.9); λ is the wavelength used in XRD (1.5418 Å); θ is the Bragg angle; β is the pure diffraction broadening of the peak at half-height that is, broadening due to the crystallite dimensions [22].

Comparison of the intensity of the XRD peaks from the two annealed samples showed that the particles obtained from the

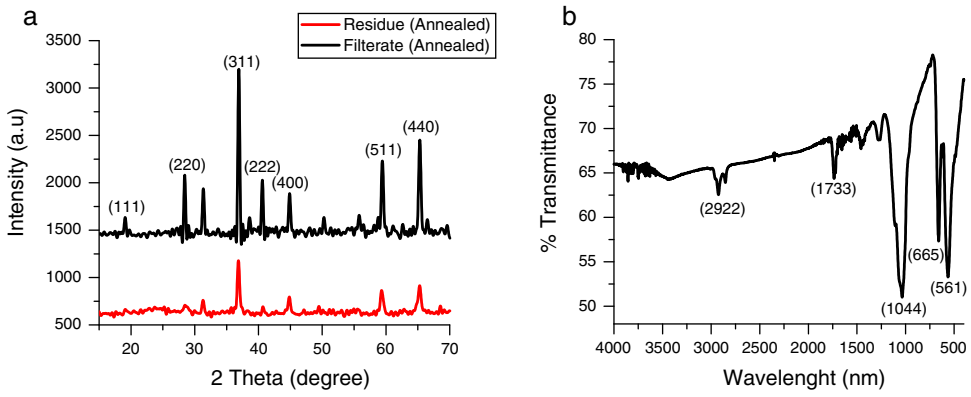

Fig. 1. (a) X-ray diffraction pattern of the as-synthesized cobalt oxide particle annealed at 500 °C; (b) FT-IR spectra of the as-synthesized cobalt oxide particles.

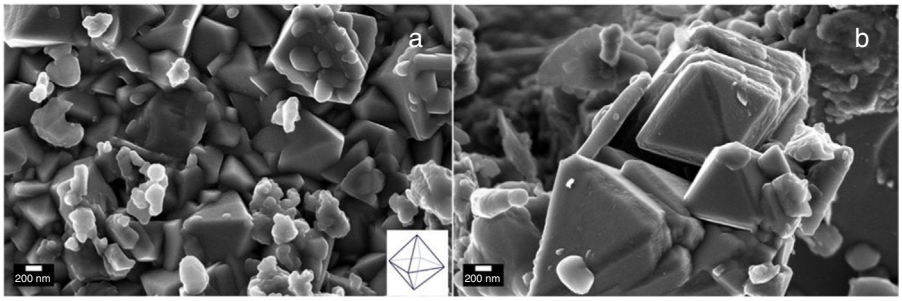

Fig. 2. (a) SEM images of hierarchical cobalt oxide mesostructures showing fracture free octahedron-like shape. (b) SEM images of mesostructure cobalt oxide particles showing the layer–layer arrangement of the supernatant.

supernatant were more crystalline than those obtained from the supernatant. This was also in agreement with the result obtained from the selected area diffraction in Fig. 4a and b. The FTIR spectrum of the prepared Co_3O_4 samples is shown in Fig. 1b. Characteristic peaks were observed at 561 and 665 cm^{-1}. These correspond to Co–O bending mode of Co_3O_4 [13]. There were also weak bands at 2922 cm^{-1} and 1733 cm^{-1}. These could indicate the presence of O-H stretching vibrations from water vapour absorption during analysis.

Electron microscopy such as Scanning electron and Transmission electron microscopy (SEM and TEM) were used to evaluate the morphology of the Co_3O_4 mesoparticles. Fig. 2a and b shows the SEM while and Fig. 3c and d shows the TEM micrographs of the as-synthesized Co_3O_4 particles annealed at 500 °C. The particles were found to be agglomerated and the relative particle sizes could not be measured. This is attributed to nucleation and crystal growth at temperature [23]. Yin and Alivisatos reported that semiconducting nanoparticles growth by thermal decomposition method takes place in many stages [24]. Firstly, the molecules of the precursors decompose and convert into complex intermediate reportedly called monomers. When this monomer exceeds the critical value, nucleating is reached by clustering of the monomers. This enables crystalline particles to grow around the nucleation sites.

The crystallinity of the as-prepared sample was improved by the annealing process. This annealing process became necessary, because, the synthesis was a facile green approach (ambient temperature). After annealing, the samples become highly crystalline as seen from the selected area electron diffraction (SAED), Fig. 3a and b. It is believed that the particle size is controlled by the reaction temperature at the initial stage of nucleation. Thus, the reaction took place at room temperature and this caused the reacting precursor to change into amorphous cobalt oxide, hence giving rise to particles with large particle size distribution and agglomeration. This observation is similar to previous report [23] where it was noted that further annealing of amorphous cobalt oxide nanoparticles with broad particle size gives rise to asymmetric particle size growth of nanocrystals with large size distribution.

The corresponding selected area electron diffraction (SAED) pattern (Fig. 4a & b) showed spot diffraction pattern indicating that the Co_3O_4 mesocrystals are arranged more or less in the same crystallographic direction. This is one of the characteristic for crystal formation via solvent-mediated mechanism. The SAED patterns consist of well-defined rings which could be indexed with face-centred cubic Co_3O_4 phase. It is important to know that no reflection of other phases was found. This is further supported by the XRD result in Fig. 1a showing the pure and single phase of Co_3O_4 mesoscale particles with regular lattice fringes as shown in Fig. 3e and f. This is further supported by the EDAX spectra in Fig. 3g and h, showing peaks corresponding to Co, and O_2. A closer look at the octahedron crystal shown in Fig. 2a and b and the SAED pattern in Fig. 3a and b obviously shows evidence of the formation of polycrystals with well-defined diffraction spots.

3.1. Self-assembled mesostructures

Previous studies have shown hierarchical nanostructured materials with basic physicochemical nature of their building blocks at different levels for high-tech applications [25]. The self-assembly of these complex architectures of cobalt particles from their dispersions at the nanoscale pivots on the competition between various forces like van der Waals, entropic, electrostatic, magnetic dipole-dipole, etc. [26,27]. In addition, the size and shape of their building blocks play a decisive role in the design of such architectures.

Recently, Li et al. [25], developed a solution based epitaxial growth method to prepare a novel crystal facet-based CeO_2 homo-junction consisting of hexahedron prism-anchored octahedron. Singh et al. reported on 2-dimensional magnetite nanocubes decorated as helical and belt superstructures on air-liquid interface formed during evaporation induced spontaneous self-assembly in the presence of an external magnetic field [28]. Murray and co-workers have demonstrated a dry-driven assembly process to fabricate large area ordering of nanocrystals without using external magnetic field [27,29]. In both studies, well-defined cubic-shaped nanoparticles were synthesized using hydrothermal method. Previous study also demonstrated the coexistence of square and hexagonally packed mesostructures arising due to structural diversity in iron oxide nanoparticles used under external magnetic field [30]. Notably, these reports were based on nanocrystals of a few nanometer sizes. Taking lead from these studies, we report for the first time, the facial green synthesis of antiferromagnetic Co_3O_4 mesoscale particles with hierarchical octahedron assemblies (Figs. 2 and 4). Here, the growth and formation of cobalt oxide mesostructures were

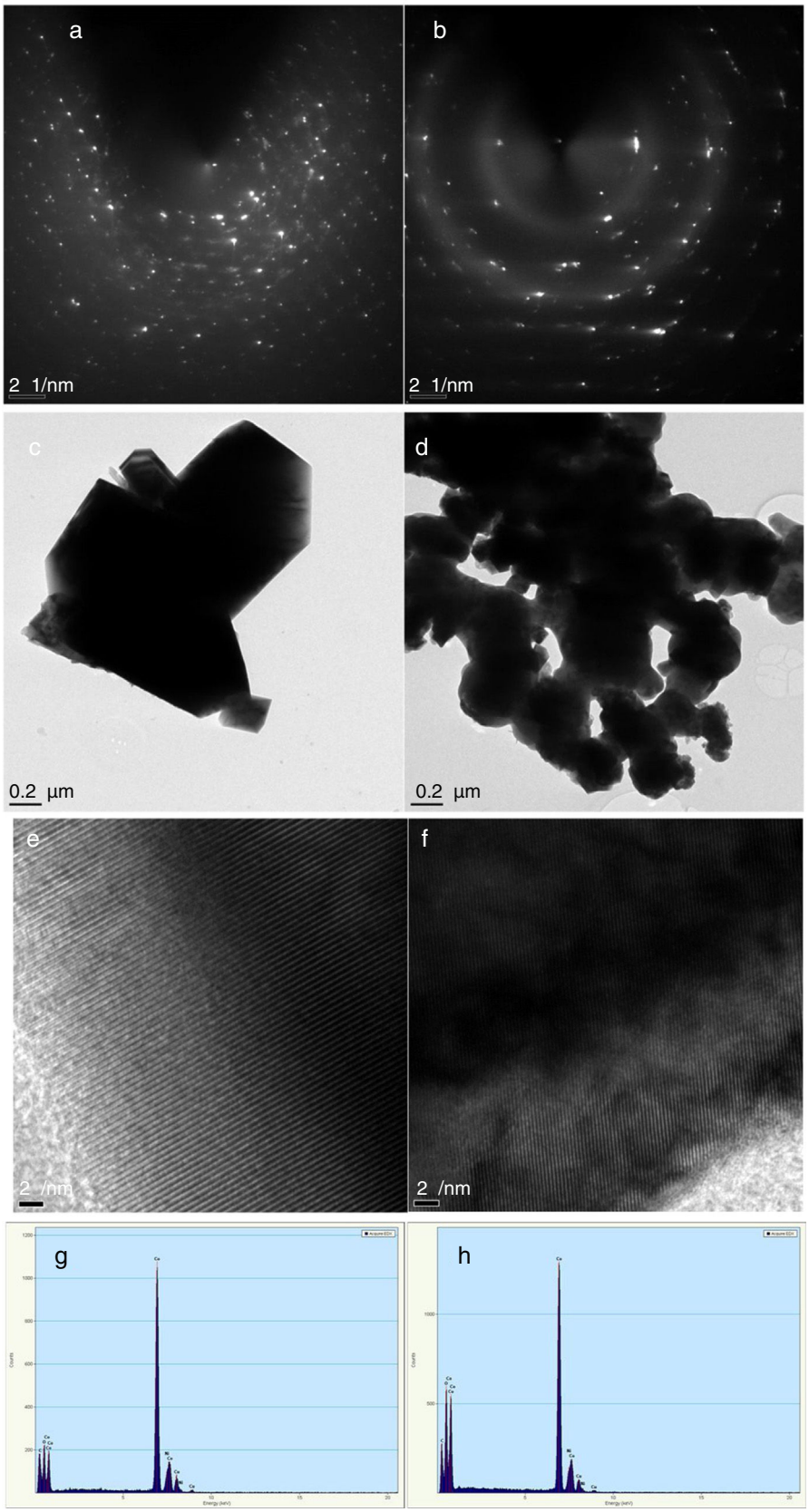

Fig. 3. Characterization of Co_3O_4 mesoscale particles synthesized by a facile green approach using *Manihot esculenta extract*. Characterization of Co_3O_4 nanoparticles synthesized by a facile green approach using *Manihot esculata extract.* (a & b) SAED patterns, (c & d,) TEM images, (e & f) lattice fringes and (g & h) EDAX spectra of the as-synthesized Co_3O_4 mesooparticles (precipitate & supernatant) annealed @ 500 °C.

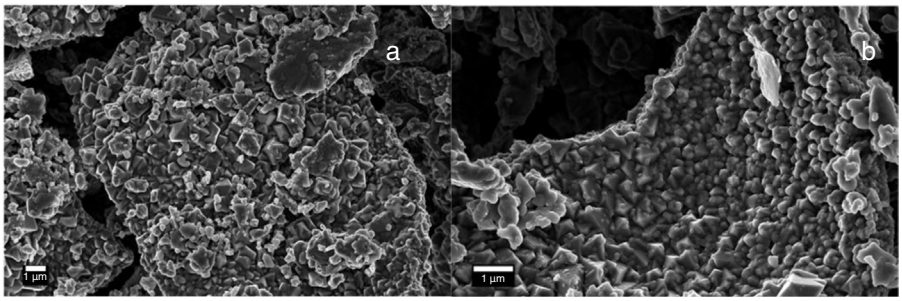

Fig. 4. SEM images of the assembled mesostructured cobalt oxide particles. a) Precipitate and b) Supernatant.

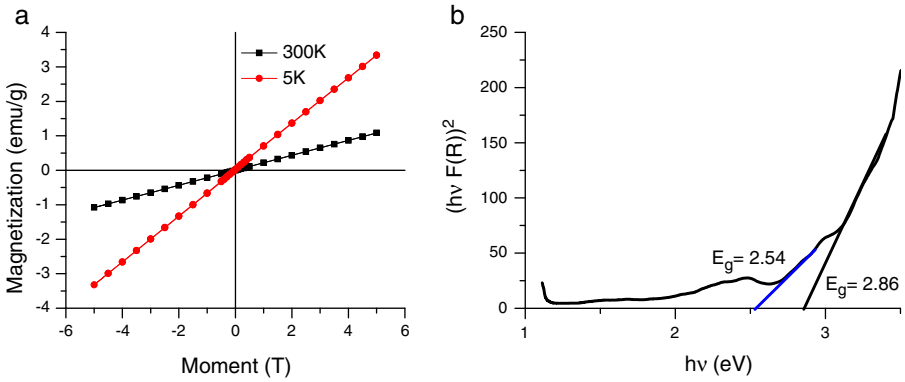

Fig. 5. (a) Saturation magnetization; (b) band gap of Co_3O_4 mesoparticles particles.

turned during synthesis by the addition of chelating agent and this process was performed at ambient temperature (Scheme 1).

3.2. Magnetic and optical properties

The magnetic hysteresis curve at 5 K and 300 K is presented in Fig. 5a. The magnetization of the samples was measured as a function of the magnetic field (H,T) at 5 K and 300 K in the applied magnetic field sweeping between ±5 T. The magnetization curve looks antiferromagnetic. This antiferromagnetic behaviour exhibited by the as-synthesized Co_3O_4 mesoscale particles is similar to antiferromagnetic behaviour of the bulk Co_3O_4. These implies that an ideal bulk antiferromagnetic Co_3O_4 exhibits magnetic moment per particle which is equal to zero. Therefore, there could be complete compensation of sub-lattice spins [15,31]. This explains the mesoscale particles size.

This implies that Co_3O_4 particles have a normal cubic spinel structure with an antiferromagnetic exchange between ions which occupy the tetrahedral and the octahedral sites [32,33]. Hence, it has zero net magnetization due to complete compensation of sub-lattice magnetization

The optical spectra of the mesostructured Co_3O_4 particles were measured on an opaque substrate Fig. 5b.

The band gap of the as-synthesized Co_3O_4 mesoparticles was evaluated using Tauc relation[34].

$$(h\upsilon\alpha)^{1/n} = A(h\upsilon - Eg) \quad (2)$$

where, h: Plank's constant, v: frequency of vibration, α: absorption coefficient, Eg: bandgap, A: proportional constant, n: denote the nature of the electronic transition of the sample which is responsible for adsorption. The values are ½, 3/2, 2 or 3. In this analysis, direct allowed electronic transition was used, therefore n was ½.

The acquired diffuse reflectance spectrum was converted to Kubelka–Munk function as the sample was measured on an opaque substrate [35]. Thus, the vertical axis was converted to $F(R\infty)$ quantity, which is proportional to absorption coefficient. Furthermore, α in the Tauc equation is replaced with $(R\infty)$, the actual relation used in the experiment becomes,

$$(h\upsilon F(r\infty))^2 = A(h\upsilon - Eg) \quad (3)$$

It is reported that bandgap varies with crystallite sizes, usually due to O^{2-}–$Co^{3+}$and O^{2}–Co^{2+} charge transfer processes [36,37]. We obtained a band gap of 2.86 eV and 2.54 eV which was slightly higher and lower than the reported bulk value (Eg = 3.17 eV and 177 eV respectively). As earlier mentioned, increase in band gap can be attributed to quantum confinement and small grain size of the Co_3O_4 mesoparticles [14,38].

4. Conclusions

This study showed that mesostructured Co_3O_4 of high industrial potentials can be synthesized by a more environmentally friendly process using the extract of *Manihot esculenta Crantz* extract as a chelating/stabilizing agent. The as-synthesized mesostructured Co_3O_4 had a prism like-anchored octahedron morphology having antiferromagnetic behaviour and a band gap of 2.86 eV and 2.54 eV respectively. It is hoped that this facile

green, more environment-friendly approach will be adopted in the synthesis of Co_3O_4 mesoparticles.

Conflict of interest

No conflict of interest was reported by the authors.

Acknowledgements

The authors are grateful to TWAS and UNESCO for their support for this research. They are also grateful to National Research Foundation – iThemba LABS, Cape Town, South Africa for hosting two of the authors (Prof. Esther Ikhuoria and Dr Stanley Omorogbe) and providing the facilities for this study.

References

[1] R. Manigandan, K. Giribabu, R. Suresh, L. Vijayalakshmi, A. Stephen, V. Narayanan, Cobalt oxide nanoparticles: characterization and its electrocatalytic activity towards nitrobenzene, Chem. Sci. Trans. 2 (2013) S47–S50.

[2] F. Chekin, S.M. Vahdat, M.J. Asadi, Green synthesis and characterization of cobalt oxide nanoparticles and its electrocatalytic behavior, Russ. J. Appl. Chem. 89 (2016) 816–822.

[3] C. Ding, F. Zhao, M. Zhang, S. Zhang, Hybridization biosensor using 2,9-dimethyl-1,10-phenantroline cobalt as electrochemical indicator for detection of hepatitis B virus DNA, Bioelectrochemistry 72 (2008) 28–33.

[4] E. Villagra, F. Bedioui, T. Nyokong, J.C. Canales, M. Sancy, M.A. Páez, et al., Tuning the redox properties of Co-N_4 macrocyclic complexes for the catalytic electrooxidation of glucose, Electrochim. Acta 53 (2008) 4883–4888.

[5] A. Diallo, A.C. Beye, T.B. Doyle, E. Park, M. Maaza, Green synthesis of Co_3O_4 nanoparticles via *Aspalathus linearis*: physical properties, Green Chem. Lett. Rev. 8 (2015) 30–36.

[6] A. Fernandez Osorio, A. Vasquez-Olmos, R. Sato-Berru, R. Escudero, Hydrothermal synthesis of co_3o_4 nanooctahedra and their magnetic properties, Rev. Adv. Mater. Sci. 22 (2009) 60–66.

[7] G. Cotton FAaW, Advanced Inorganic Chemistry: A Comprehensive Text, Interscience Publishers, John Wiley & Sons, New York, 1980.

[8] U. Lagerqvist, M. Ottosson, A. Pohl, Synthesis and characterization of cobalt oxide and composite thin films, Adv. Mater. 3 (2014) 52–57.

[9] M.U. Sankar, S. Aigal, S.M. Maliyekkal, A. Chaudhary, Anshup, A.A. Kumar, et al., Biopolymer-reinforced synthetic granularnanocomposites for affordable point-of-use water purification, PNAS 110 (2013) 8459–8464.

[10] S.L. Sharifi, H.R. Shakur, A. Mirzaei, A. Salmani, M.H. Hosseini, Characterization of cobalt oxide Co_3O_4 nanoparticles prepared by various methods: effect of calcination temperatures on size, dimension and catalytic decomposition of hydrogen peroxide, Int. J. Nanosci. Nanotechnol. 9 (2013) 51–58.

[11] M.T. Makhlouf, B.M. Abu-Zied, T.H. Mansoure, Direct fabrication of cobalt oxide nanoparticles employing sucrose as a combustion fuel, J. Nanoparticles 2013 (2013) 7.

[12] C.J. Denis, C.J. Tighe, R.I. Gruar, N.M. Makwana, J.A. Darr, Nucleation and growth of cobalt oxide nanoparticles in a continuous hydrothermal reactor under laminar and turbulent flow, Cryst. Growth Design 15 (2015) 4256–4265.

[13] Y. Teng, S. Yamamoto, Y. Kusano, M. Azuma, Y. Shimakawa, One-pot hydrothermal synthesis of uniformly cubic Co_3O_4 nanocrystals, Mater. Lett. 64 (2010) 239–242.

[14] R.V. Kumar, Y. Diamant, A. Gedanken, Sonochemical synthesis and characterization of nanometer-size transition metal oxides from metal acetates, Chem. Mater. 12 (2000) 2301–2305.

[15] E.M.M. Ibrahim, L.H. Abdel-Rahman, A.M. Abu-Dief, A. Elshafaie, S.K. Hamdan, A.M. Ahmed, Electric, thermoelectric and magnetic characterization of γ-Fe_2O_3 and Co_3O_4 nanoparticles synthesized by facile thermal decomposition of metal-Schiff base complexes, Mater. Res. Bull. 99 (2018) 103–108.

[16] M. Shah, D. Fawcett, S. Sharma, S.K. Tripathy, G.E. Jai Poinern, Green synthesis of metallic nanoparticles via biological entities, Materials 8 (2015) 7278–7308.

[17] B.T. Sone, E. Manikandan, A. Gurib-Fakim, M. Maaza, Single-phase α-Cr_2O_3 nanoparticles' green synthesis using *Callistemon viminalis*' red flower extract, Green Chem. Lett. Rev. 9 (2016) 85–90.

[18] S.H. Katz, W.W. Weaver, Encyclopedia of Food and Culture, Schribner, New York, 2003.

[19] J. Sulistyo, L.J. Shya, H. Mamat, N.A. Wahab, Nutritional value of fortified cassava flour prepared from modified cassava flour and fermented protein hydrolysates, AIP Conf. Proc. 1744 (2016) 020030.

[20] O.A. Emmanuel, A. Clement, S.B. Agnes, L. Chiwona-Karlton, B.N. Drinah, Chemical composition and cyanogenic potential of traditional and high yielding CMD resistant cassava (*Manihot esculenta Crantz*) varieties, Int. Food Res. J. 19 (2012) 175–181.

[21] D. Siritunga, R.T. Sayre, Generation of cyanogen-free transgenic cassava, Planta 217 (2003) 367–373.

[22] M. Salavati-Niasari, N. Mir, F. Davar, Synthesis and characterization of Co_3O_4 nanorods by thermal decomposition of cobalt oxalate, J. Phys. Chem. Solids 70 (2009) 847–852.

[23] R.K. Gupta, A.K. Sinha, B.N. Raja Sekhar, A.K. Srivastava, G. Singh, S.K. Deb, Synthesis and characterization of various phases of cobalt oxide nanoparticles using inorganic precursor, Appl. Phys. A 103 (2011) 13–19.

[24] Y. Yin, A.P. Alivisatos, Colloidal nanocrystal synthesis and the organic–inorganic interface, Nature 437 (2005) 664–670.

[25] P. Li, Y. Zhou, Z. Zhao, Q. Xu, X. Wang, M. Xiao, et al., Hexahedron prism-anchored octahedronal CeO_2: crystal facet-based homojunction promoting efficient solar fuel synthesis, J. Am. Chem. Soc. 137 (2015) 9547–9550.

[26] R.K. Pai, S. Pillai, Water-soluble terpolymer directs the hollow triangular cones of packed calcite needles, Cryst. Growth Design 7 (2007) 215–217.

[27] Y. Lalatonne, J. Richardi, M.P. Pileni, Van der Waals versus dipolar forces controlling mesoscopic organizations of magnetic nanocrystals, Nat. Mater. 3 (2004) 121–125.

[28] G. Singh, H. Chan, A. Baskin, E. Gelman, N. Repnin, P. Král, et al., Self-assembly of magnetite nanocubes into helical superstructures, Science 345 (2014) 1149–1153.

[29] A. Dong, J. Chen, S.J. Oh, Koh W-k, F. Xiu, X. Ye, et al., Multiscale periodic assembly of striped nanocrystal superlattice films on a liquid surface, Nano Lett. 11 (2011) 841–846.

[30] S. Disch, E. Wetterskog, R.P. Hermann, D. Korolkov, P. Busch, P. Boesecke, et al., Structural diversity in iron oxide nanoparticle assemblies as directed by particle morphology and orientation, Nanoscale 5 (2013) 3969–3975.

[31] E.M.M. Ibrahim, A.M. Abu-Dief, A. Elshafaie, A.M. Ahmed, Electrical, thermoelectrical and magnetic properties of approximately 20-nm Ni–Co–O nanoparticles and investigation of their conduction phenomena, Mater. Chem. Phys. 192 (2017) 41–47.

[32] S. Farhadi, K. Pourzare, S. Sadeghinejad, Simple preparation of ferromagnetic Co_3O_4 nanoparticles by thermal dissociation of the $[CoII(NH_3)_6](NO_3)_2$ complex at low temperature, J. Nanostruct. Chem. 3 (2013) 16.

[33] Y. Ichiyanagi, Y. Kimishima, S. Yamada, Magnetic study on Co_3O_4 nanoparticles, J. Magnet. Magnet. Mater. (2004) 272-276, supplement: E1245–E6.

[34] J. Tauc, Optical properties of amorphous semiconductors, in: J. Tauc (Ed.), Amorphous and Liquid Semiconductors, Springer US, Boston, MA, 1974, pp. 159–220.

[35] R. López, R. Gómez, Band-gap energy estimation from diffuse reflectance measurements on sol–gel and commercial TiO_2: a comparative study, J. Sol-Gel Sci. Technol. 61 (2012) 1–7.

[36] A.B. Murphy, Band-gap determination from diffuse reflectance measurements of semiconductor films, and application to photoelectrochemical water-splitting, Solar Energy Mater. Solar Cells 91 (2007) 1326–1337.

[37] A.K. Sarfraz, S.K. Hasanain, Size dependence of magnetic and optical properties of Co_3O_4 nanoparticles, Acta Phys. Pol. A 125 (2014) 139–144.

[38] A. Gulino, P. Dapporto, P. Rossi, I. Fragalà, A novel self-generating liquid MOCVD precursor for Co_3O_4 thin films, Chem. Mater. 15 (2003) 3748–3752.